

Monitoring a single ion's motion by second-order photon correlations

D Rotter^{1,3}, M Mukherjee¹, F Dubin¹ and R Blatt^{1,2}

¹ Institute for Experimental Physics, University of Innsbruck, Technikerstrasse 25, A-6020 Innsbruck, Austria

² Institute for Quantum Optics and Quantum Information of the Austrian Academy of Sciences, Otto-Hittmair-Platz 1, 6020 Innsbruck, Austria
E-mail: Daniel.Rotter@uibk.ac.at

New Journal of Physics **10** (2008) 043011 (9pp)

Received 22 January 2008

Published 10 April 2008

Online at <http://www.njp.org/>

doi:10.1088/1367-2630/10/4/043011

Abstract. For a single trapped ion, second-order time correlations of fluorescence photons are measured in a self-homodyne configuration by beating the fluorescence with itself. At the nanosecond timescale, the correlations are governed by electronic excitation and decay of the ion and anti-bunching in the resonance fluorescence is observed and quantitatively reproduced. On the other hand, at the microsecond timescale the motion of the ion determines the correlations: secular motional modes, their amplitude and relative coherence are measured. Besides precisely monitoring the trap frequencies, our observations also quantify the temporal stability of the trapping potential.

Contents

1. Introduction	2
2. Experimental set-up	3
3. Theoretical model	4
4. Data acquisition	5
5. Experimental results	6
6. Summary and conclusion	7
Acknowledgments	9
References	9

³ Author to whom any correspondence should be addressed.

1. Introduction

Trapped ions are well known and widely used for precision experiments, such as for example, for time and frequency standard applications where they appear to be ideal candidates (see [1] and references therein): a single trapped ion can indeed be laser cooled and well prepared in the ground state of the respective trapping potential such that any residual perturbation due to the ion's motion can be minimized. With such control and the ability to produce almost arbitrary quantum states of motion [2], throughout the last decade, single trapped ions and strings of ions have become ideal objects for the new field of quantum information processing where individual ions serve as the memory for quantum information and allow one to perform quantum information processing experiments. In addition, single ions have been increasingly used for fundamental investigations in quantum optics, for example, as single [3] or two-photon sources [4, 5], for basic investigations of resonance fluorescence and even for quantum feedback experiments [6], where the motion of an ion can be influenced via back-action of a single emitted photon on the radiating dipole. For all of these applications, it is important to monitor a single ion's residual motion as fast as possible and thus to precisely control both the trapping parameters and the ion's motional state.

Fluorescence photons emitted by a single atom carry information about both the states of the valence electron and the motional states of the center of mass of the atom, i.e. the internal and external degrees of freedom of the atomic wavefunction [2]. The internal dynamics is known to be characterized by the temporal distribution of the emitted fluorescence photons, usually analyzed by the second-order correlation function

$$g^{(2)}(t, t+T) = \frac{\langle : I(t)I(t+T) : \rangle}{|\langle I(t) \rangle|^2}, \quad (1)$$

where $I(t)$ denotes the intensity operator at time t and T is the delay between any two considered photons⁴. The quantum nature of the radiation emitted by a single atom is revealed in the correlation function by so-called anti-bunching, i.e. $g^{(2)} = 0$ at $T = 0$. Clearly, the Cauchy–Schwarz inequality, i.e. the physical law of classical fields, is violated [7]. In fact, resonance fluorescence exhibits sub-Poissonian emission statistics [8] for time intervals T smaller than the lifetime of the excited state of the atom. On the other hand, when fluorescence photons are correlated at time intervals T much greater than the lifetime of the considered electronic transition, the $g^{(2)}$ -function is constant and equal to one: the distribution of photon emissions then exhibits Poissonian statistics. However, for a single trapped ion, a sinusoidal modulation of the $g^{(2)}$ -function was observed in this regime [9]. This was attributed to the trap's radiofrequency driven motion (micro-motion) while contributions from oscillations in the pseudo-potential of the trap (secular motion) were not observed. These oscillations appear on a longer timescale and were reported in other experiments [10, 11] performed outside the Lamb–Dicke regime [2] where motional sidebands are dominant in the fluorescence spectrum.

In the Lamb–Dicke regime, the conventional approach to characterizing single-ion motional states relies on spectroscopic analysis of motional sidebands. A detailed description of the existing protocols to reconstruct the motional density matrix or the Wigner function can be found in [2] and references therein. A diagnostic test for quantum effects of motion for a single trapped ion was recently proposed [12], using second-order correlations of the emitted photons. However, to our best knowledge the latter has not been implemented yet.

⁴ Operators inside colons are time and normally ordered.

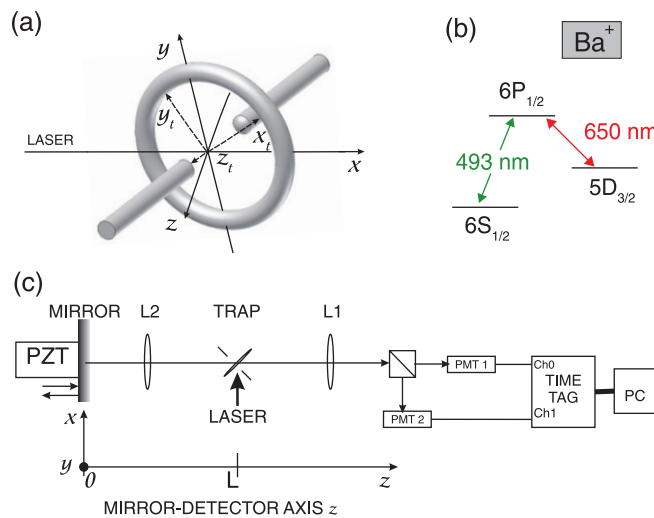


Figure 1. (a) Geometry of the trap with its principal axes (x_t , y_t , z_t) determined by the secular motion in three directions. The angles between these axes and the laser propagation direction are (60° , 60° and 45°), respectively. (b) Relevant atomic levels of the $^{138}\text{Ba}^+$ ion. (c) Experimental set-up: the average distance between the trap and the mirror is set to $L \approx 25$ cm. Lens L2 has a numerical aperture 0.4 and collects the fluorescence photons. Single photons are detected by the photomultipliers PMT1 and PMT2, time tagging of the individual photon counts is obtained via the TAG with ≈ 100 ps time resolution. The mirror is mounted on a piezo-translation stage (PZT) to adjust the phase of the homodyne signal.

Below, we demonstrate that the residual motion of a single trapped ion in the Lamb–Dicke regime can be characterized without performing demanding sideband spectroscopy. In a self-homodyne configuration, we show that the second-order correlation function allows one to characterize the secular motion of a trapped ion. In particular, we report photon correlations which are modulated at long time intervals T by a beating between the two radial modes of motion of the ion in the trap. The amplitude of the beat signal is controlled by the amplitude of the corresponding secular motional modes. This allows us to deduce the mean occupation number of the ion motional states, $n \approx 17$, in agreement with independent measurements performed previously [6]. Furthermore, the beat signal quantifies the dephasing time between the radial modes at the Doppler limit, as 1.64 ms for our trap. Moreover, the short-time anti-bunching of the emitted fluorescence is also quantified in our experiments. Our measurements in fact reveal in a single record the dynamics of both internal and external degrees of freedom of the ion’s wavefunction, ranging from nanosecond to millisecond timescales.

2. Experimental set-up

The experimental set-up and a partial energy level diagram for the $^{138}\text{Ba}^+$ ion are shown in figure 1. The spherical Paul trap is driven with a radio frequency of 20 MHz applied to the ring electrode while the endcaps are grounded. This results in trap frequencies of about 1, 1.2

and 2 MHz for the two radial (x_t and y_t) and axial (z_t) modes of motion, respectively. The non-degeneracy in the radial modes arises from a small asymmetry of the quadrupole potential in the azimuthal plane. A narrow band (20–50 kHz) tunable diode laser at 493 nm (green) drives the $S_{1/2}$ – $P_{1/2}$ transition which is used for laser cooling and the observation of the resonance fluorescence. Another narrow band laser at 650 nm (red) pumps the ion back to the cooling cycle via the $D_{3/2}$ – $P_{1/2}$ transition. The lasers have frequencies close to the respective resonances and intensities below saturation.

In the following, we study the green part (i.e. at $\lambda = 493\text{nm}$) of the resonance fluorescence. A fraction $\epsilon = 1.5\%$ of that is collimated by a 0.4 numerical aperture lens with small wave front aberrations (less than $\lambda/5$) (L2 in figure 1) and sent to a retro-reflecting mirror situated $L \approx 25\text{ cm}$ away from the ion. Upon reflection the fluorescence is then focused back onto the ion with high spatial precision using piezo-mechanical mounts for the mirror. Along the mirror–detector axis, green fluorescence photons can thus take two indistinguishable paths before impinging on the photo-detectors: either they are emitted directly towards the detectors or they are emitted towards the mirror and then detected after reflection. The distance between the ion and the mirror sets the time delay, $\tau = 2 \times L/c \approx 1.5\text{ ns}$, between these paths. This leads to a single photon interference of the green fluorescence as L is varied, with a visibility as high as 72% for very weak laser excitation [13]. The analysis presented in the following was obtained for slightly higher excitation, thus the visibility reduces to 38%. With this interference setup, we accurately measure the variations of the ion–mirror distance, L , because any residual motion modifies L and thus the level of (the interfering) fluorescence we detect. Using a mean photo-current as set-point, the average value of L is fixed (on a timescale of seconds) in our experiments such that the ion is located at the slope of the standing wave pattern that results from the interfering fluorescence paths. Thus, on average and for long timescales the mirror position is controlled with a precision of 10 nm, limited by the noise in the servo loop stabilizing the piezo-mechanical positioning. On the other hand, the faster motion of the ion (timescale of $\approx 1\ \mu\text{s}$) is revealed by the modulation it induces on the mean photocurrent.

3. Theoretical model

To obtain quantitative results, we investigate the second-order correlation function for the green fluorescence photons ($\lambda = 493\text{ nm}$), as given by the experimental set-up.

We denote the mirror–detector axis as z (see figure 1). The mirror is placed at $z = 0$, the center of the trap is at $z = L$ and we write the position of the ion relative to the center of the trap, $\hat{z}_m \propto (a_m + a_m^\dagger)$, with a_m and a_m^\dagger the bosonic operators associated with the motion of the ion. The trap axis is slightly tilted with respect to z ; z_m can in fact correspond to the projection of x_t , y_t and z_t along z (x_t , y_t and z_t denote the coordinates of the ion in the basis of the trapping potential, see figure 1). Along the z -axis, the field operator for green fluorescence then reads

$$E_z(t) = \sqrt{\epsilon\Gamma_G} \sin(k_G(L + \hat{z}_m))\sigma^-(t) + E_{in}(t), \quad (2)$$

where Γ_G is the spontaneous emission rate of the $P_{1/2}$ – $S_{1/2}$ transition and k_G denotes the corresponding k -vector at 493 nm [6]. In equation (2), $\sigma^- = |S_{1/2}\rangle\langle P_{1/2}|$ is the lowering Pauli operator, associated with the creation of a photon, and E_{in} represents the input state of the mirror mode for a measurement at time t [14]. In the following, we consider a white noise input and then introduce $\langle E_{in}(t')E_{in}(t) \rangle = \bar{N}\delta(t' - t)$, with the mean number \bar{N} of input counts. Moreover,

when writing equation (2) we have implicitly assumed that our experiments are carried out in the Markovian limit (non-Markovian behavior is observed for time delays that are comparable to the internal timescales of the ion and is reported in [15]). The time delay induced by the mirror, τ , is in fact smaller than the internal dynamics of the system, given by the lifetime of the $P_{1/2}$ state, $\tau \ll 1/\Gamma_G$, and the timescales associated with ion–laser interactions, $\tau \ll 1/\Omega$, $1/|\Delta_L|$, with the Rabi frequency Ω and the detuning Δ_L , respectively. Along the z -axis, the second-order correlation function is defined by

$$g_z^{(2)}(t, t+T) \propto \langle E_z^\dagger(t) E_z^\dagger(t+T) E_z(t+T) E_z(t) \rangle. \quad (3)$$

For our experimental setup, the mean occupation number of motional states at the Doppler limit, $n \sim \langle a_m^\dagger a_m \rangle$, was previously deduced to be $n \approx 17$ [6]. In the following measurements, we apply similar laser-cooling yielding the same average quantum number $n \approx 17$, i.e. $\eta\sqrt{n} \approx 0.3$. $\eta = 2\pi a_0/\lambda \sim 0.07$ is the Lamb–Dicke parameter, a_0 denotes the rms size of the trap ground state. In this Lamb–Dicke regime, the secular motional sidebands have intensities reduced by the effective Lamb–Dicke parameter, relative to the elastic component of the fluorescence. We can thus expand exponentials, e.g. $e^{ik_G \hat{z}_m} \equiv 1 + i\eta(a_m + a_m^\dagger) + o(\eta^2)$. For the ion placed at the slope of the mirror standing wave, i.e. $k_G L = \pi/4$ [π], equation (2) becomes

$$E_z(t) = \sqrt{\epsilon \Gamma_G \hat{c}_m} \sigma^-(t) + E_{in}(t), \quad (4)$$

with

$$\hat{c}_m = \frac{1}{\sqrt{2}} \left(1 + \eta(a_m + a_m^\dagger) - \frac{\eta^2}{2} (a_m + a_m^\dagger)^2 \right). \quad (5)$$

From equations (2)–(5) the deduced normalized second-order correlation function is

$$g_z^{(2)}(t, t+T) \cong (1 + 2\eta \langle a_m + a_m^\dagger \rangle) g^{(2)}(t, t+T) + 2 \frac{\bar{N}}{\bar{I}}, \quad (6)$$

where $g^{(2)}(t, t+T)$ denotes the usual normalized $g^{(2)}$ -function for a single ion at rest. In order to accurately reproduce the exact shape of the measured correlations, $g^{(2)}$ is evaluated considering the eight relevant electronic levels for the ion internal states [16]. In equation (6), \bar{I} is the mean fluorescence intensity, the last term in fact corresponds to accidental correlations (contributions negligible with respect to $\frac{\bar{N}}{\bar{I}}$ are not shown for clarity). The second term, proportional to $\langle a_m + a_m^\dagger \rangle$, shows that the $g^{(2)}$ -function is modulated by the motion of the ion.

As previously mentioned, every mode of motion contributes to \hat{z}_m . The second term in equation (6) in fact sums contributions induced by the two radial and the axial modes, as well as the residual micro-motion, such that the $g^{(2)}$ -function should in principle show a beating between all motional frequencies. The amplitude of the beat signal is controlled by the projection of the axial and radial axes along z , but also by the corresponding amplitudes of motion along these directions. Hence, $g_z^{(2)}$ quantifies the mean occupation number of the ion's motional states. Furthermore, as for any beat signal, the relative phase coherence between the motional modes is also revealed. Finally, for our continuous laser excitation, equation (6) is evaluated at steady state, i.e. for $t \rightarrow \infty$, such that $g_z^{(2)}(t, t+T) \rightarrow g_z^{(2)}(T)$.

4. Data acquisition

In the experiment presented here, the mirror position with respect to the ion is fixed such that the emitted fluorescence level always stays at the slope of the single-photon interference fringe.

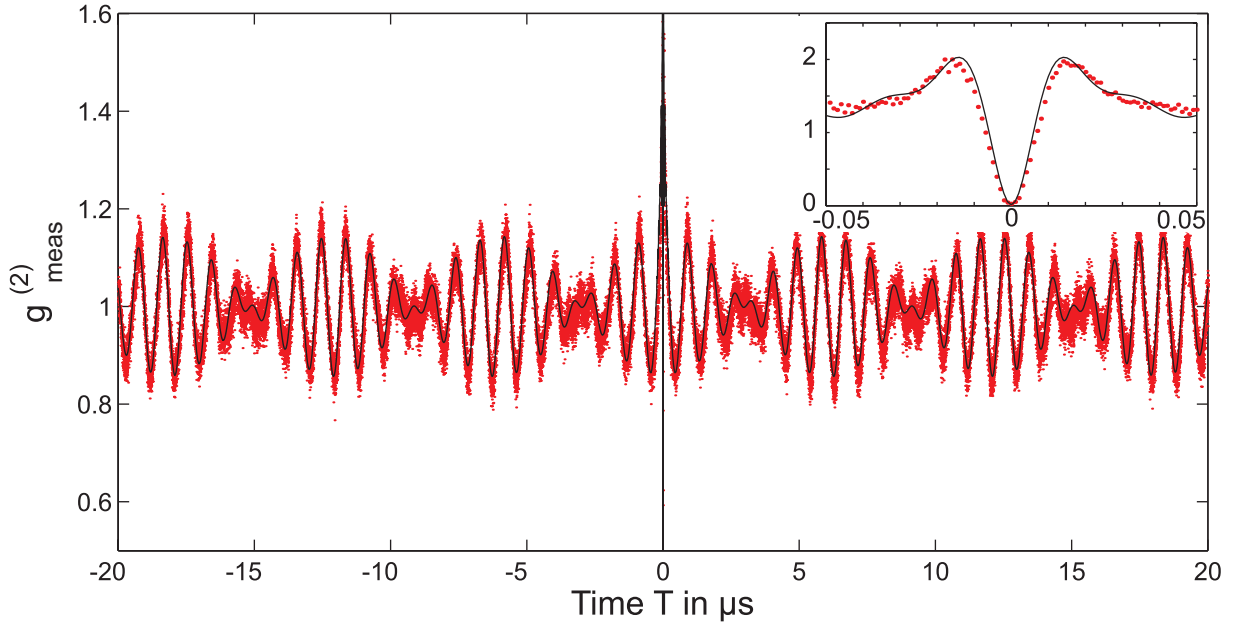


Figure 2. Second-order correlation function for time intervals T up to $20 \mu\text{s}$: the experimental data are shown as (red) dots. The theoretical prediction for the same experimental parameters and for $n = 17$ and $V = 38\%$ is presented as a black solid line. The modulation of the $g^{(2)}$ -function reveals the two frequencies of the motional sidebands along the radial directions. Inset: photon antibunching for short times T up to 50 ns . Experimental data are displayed with a time resolution of 1 ns .

The photons detected by the two photomultipliers are time tagged according to their arrival time in an auto correlator (TAG in figure 1). Second-order time correlations among these events are then calculated. Unlike methods where merely time intervals between *successively* detected photons are correlated, the time tag method has no statistical influence on the count rate (pile-up effect) and needs no systematic corrections [17]. Finally, accidental correlations, e.g. the last term in equation (6), are subtracted and the second-order correlation function is normalized.

5. Experimental results

In figure 2, we present the measured second-order photon correlation function. The overlap of the direct fluorescence with its image created by the mirror reflection is not perfect: we measure a single-photon interference visibility, $V \approx 38\%$. Hence, a mixture of interacting and non-interacting correlations is observed. These have respective weights governed by the interference contrast, yielding a measured correlation function, $g_{\text{meas}}^{(2)}(T) = Vg_z^{(2)}(T) + (1 - V)g_{\text{ni}}^{(2)}(T)$, where the last part describes the non-interfering term. It induces three delayed correlation functions, centered at $T = 0$ and $T = \pm\tau$ respectively, such that $g_{\text{ni}}^{(2)}(T) = (2g^{(2)}(T) + g^{(2)}(T + \tau) + g^{(2)}(|T - \tau|))/4$ (details can be found in [4, 15]). In figure 2, we only correct the correlation function for accidental correlations. Let us now discuss the coherent part of the interaction between directly emitted and reflected fluorescence photons, i.e. the signal described by equation (6).

Apart from the usual photon anti-bunching, for time intervals T greater than $1/(2\pi\Gamma_G)$, we resolve the previously mentioned modulation in the $g^{(2)}$ -function. It clearly shows slow and fast frequency components, at $\omega_-/2\pi = 164(1)$ kHz and $\omega_+/2\pi = 2.242(2)$ MHz. Faster oscillations at the trap drive frequency (≈ 20 MHz) are not resolved. From that we conclude that micro-motion is negligible in our experiments. In fact, we operate in the most stable trap region by applying suitable voltages to compensation electrodes: the ion is thereby positioned at the minimum of the trapping potential which suppresses micro-motion. On the other hand, secular modes of motion can all contribute to the beat of the correlation function.

For our geometry (see figure 1), the axial and radial modes have angles of approximately 45° and 60° with respect to the laser axis. Therefore, laser cooling is more efficient along the axial direction z_t than along the radial ones. Hence, we expect that the modulation of the correlation function is essentially governed by the beating between the radial modes of motion. The Fourier transform of the correlation function, shown in figure 3, confirms this geometric argument. It exhibits two main lines, at $f_x = \omega_x/2\pi = 1.034(1)$ MHz and $f_y = \omega_y/2\pi = 1.198(1)$ MHz, which correspond to the motional frequencies along the x_t and y_t directions respectively. On the other hand, other frequency components, e.g. the one corresponding to the motion along z_t , are suppressed by two orders of magnitude. From the amplitude of the modulation in the correlation function, we now deduce the mean occupation number for motional states at the Doppler limit. In equation (6), we only consider contributions of the radial modes of motion which have the same projection along z . In figure 2, the result of our model is presented for $n = 17$ and $V = 38\%$. The very good agreement with the experimental observations then confirms previous measurements of the mean occupation of motional states at the Doppler limit for our experimental set-up [6]. Please also note that the theoretical prediction shown in figure 2 is obtained with the above stated frequencies, ω_x and ω_y , for the radial modes of motion.

We moreover observe a de-phasing between the radial modes of motion of the ion. The amplitude of the beat signal presented in figure 2 diminishes exponentially with a time constant of 1.64 ms. This reveals that the phase of each radial mode diffuses due to laser cooling. Such observation is confirmed by independent measurements of radial sidebands [18, 19]. On the other hand, we also observe that the central frequencies of the two radial modes do not drift within our experimental precision. More precisely, up to $T \approx 500 \mu\text{s}$, we do not resolve a difference between the frequencies used in our model and the ones of the radial modes deduced from the correlation function: figure 3 demonstrates good agreement between the data and the theoretical predictions for $T \approx 160 \mu\text{s}$. Our analysis in fact yields an upper limit for the frequency drift of the trap potential, about 2 kHz for the 30 min measurement time. Note that measurements performed with the same trap show similar drifts of the radial frequencies, on the order of 600 Hz per 30 min [18].

6. Summary and conclusion

In summary, we have shown that second-order correlations performed in a self-homodyne configuration can reveal both internal and external dynamics of a single trapped-ion. At short time intervals between photon emissions (nanoseconds), the ion internal dynamics governs the correlation function while for longer time intervals (microseconds), the motion of the ion modulates the correlation function. This allows one to deduce the remaining amplitude of motion at the Doppler limit. Furthermore the ion probes its surrounding potential such that the $g^{(2)}$ -function can also be used to characterize the stability of the trap potential.

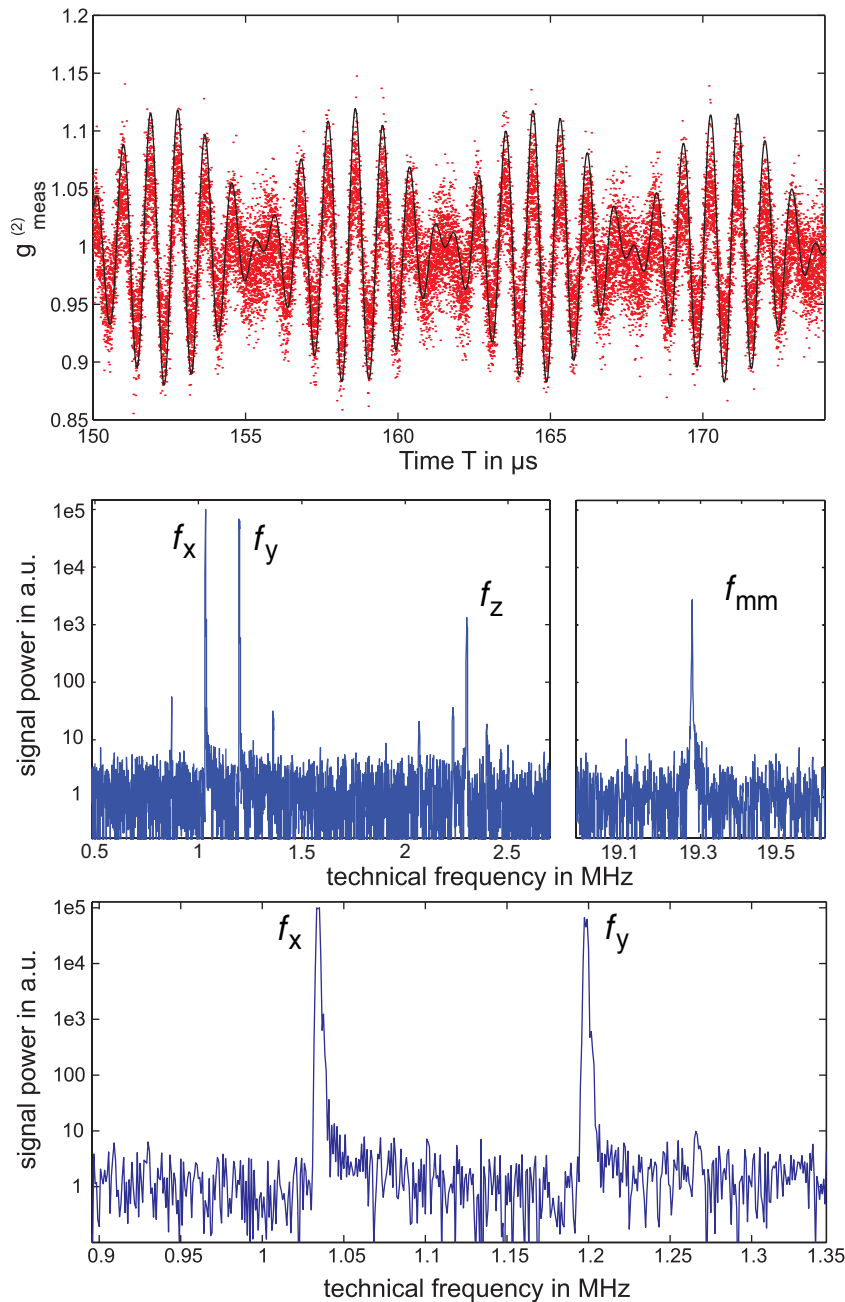


Figure 3. Top: second-order correlation function for $T \approx 160 \mu\text{s}$. Data (red points) and theoretical predictions still coincide thus revealing high trap stability (experimental data are displayed with 1 ns time resolution). Middle: spectrum of the correlation function showing the axial and radial sidebands, at the frequencies $f_x = 1.034(1)$ MHz, $f_y = 1.198(1)$ MHz and $f_z = 2.298(2)$ MHz, as well as the remaining micro-motion sideband at the trap drive frequency f_{mm} . Other visible frequency components correspond to sum/difference of the secular frequencies. Bottom: zoom of the spectrum highlighting the two radial sidebands.

To conclude, let us raise one possible implication of these experimental observations in the context of single ions trapped in a high finesse resonator. In such systems, due to the large stimulated emission of photons in the cavity mode, additional cooling of the motion of the ion should occur [20]–[22]. An experimental observation of the latter appears accessible from the second-order time correlations of the cavity output photons. Usually, photons in the cavity mode exhibit a long lifetime and the cavity acts as a low-pass filter. Hence, individual motional modes of the ion cannot be directly observed, however, if the radial motional modes have non vanishing projections along the cavity axis a slow beating in the correlation function should be observed. As in our experiments, the amplitude of the beat signal allows one to quantify the amplitude of the motion of the ion, i.e. the efficiency of cooling.

Acknowledgments

This work has been supported by the Austrian Science Fund (FWF) in the project SFB15 and M889-N02, by the European Commission (QUEST network, HPRNCT-2000-00121, QUBITS network, IST-1999-13021, SCALA Integrated Project, Contract no. 015714), and by the ‘Institut für Quanteninformation GmbH’.

References

- [1] Diddams S, Bergquist J, Jefferts S and Oates C 2004 *Science* **306** 1318
- [2] Leibfried D, Blatt R, Monroe C and Wineland D 2003 *Rev. Mod. Phys.* **75** 281
- [3] Keller M, Lange B, Hayasaka K, Lange W and Walther H 2004 *Nature* **431** 1075
- [4] Dubin F, Rotter D, Mukherjee M, Gerber S and Blatt R 2007 *Phys. Rev. Lett.* **99** 183001
- [5] Maunz P, Moehring D, Olmschenk S, Younge K, Matsukevich D and Monroe C 2007 *Nat. Phys.* **3** 538
- [6] Bushev P, Rotter D, Wilson A, Dubin F, Becher C, Eschner J, Blatt R, Steixner V, Rabl P and Zoller P 2006 *Phys. Rev. Lett.* **96** 043003
- [7] Mandel L and Wolf E 1995 *Optical Coherence and Quantum Optics* (New York: Cambridge University Press)
- [8] Briegel H-J, Meyer G M and Englert B-G 1996 *Europhys. Lett.* **33** 515
- [9] Diedrich F and Walther H 1987 *Phys. Rev. Lett.* **58** 203
- [10] Bluemel B, Kappler C, Quint W and Walther H 1989 *Phys. Rev. A* **40** 808
- [11] Dholakia K, Horvath G Zs K, Segal D M, Thompson R C, Warrington D M and Wilson D C 1993 *Phys. Rev. A* **47** 441
- [12] Jakob M and Kryuchkyan G Yu 1999 *Phys. Rev. A* **59** 2111
- [13] Eschner J, Raab Ch, Schmidt-Kaler F and Blatt R 2001 *Nature* **413** 495
- [14] Gardiner C W and Zoller P 2004 *Quantum Noise* (Berlin: Springer)
- [15] Dubin F, Rotter D, Mukherjee M, Russo C, Eschner J and Blatt R 2007 *Phys. Rev. Lett.* **98** 183003
- [16] Schubert M, Siemers I, Blatt R, Neuhauser W and Toschek P 1995 *Phys. Rev. A* **52** 2994
- [17] Coates P B 1968 *J. Phys. E: Sci. Instrum.* **1** 878
- [18] Bushev P, Wilson A, Eschner J, Raab C, Schmidt-Kaler F, Becher C and Blatt R 2004 *Phys. Rev. Lett.* **92** 223602
- [19] Raab Ch, Eschner J, Bolle J, Oberst H, Schmidt-Kaler F and Blatt R 2000 *Phys. Rev. Lett.* **85** 538
- [20] Salzburger T and Ritsch H 2004 *Phys. Rev. Lett.* **93** 063002
- [21] Maunz P, Puppe T, Schuster I, Syassen N, Pinkse P W H and Rempe G 2004 *Nature* **428** 50
- [22] Boozer A D, Boca A, Miller R, Northup T E and Kimble H J 2006 *Phys. Rev. Lett.* **97** 083602